Journal of Polymer Science

WILEY

JOURNAL OF POLYMER SCIENCE

RESEARCH ARTICLE OPEN ACCESS

Low T_g PLA-Based Copolymer Foams for Tissue Engineering Applications: Influence of Supercritical CO_2 and N_2 Mixtures on Open-Cell Content, Morphology, and Storage Stability

Annalena Pongratz[1] | Marcel Dippold[1] | Svenja Reimer[2] | Oliver Heß[2] | Holger Ruckdäschel[1]

[1]University of Bayreuth, Department of Polymer Engineering, Bayreuth, Germany | [2]PolyMedics Innovations GmbH, Kirchheim unter Teck, Germany

Correspondence: Holger Ruckdäschel (holger.ruckdaeschel@uni-bayreuth.de)

Received: 14 November 2024 | **Revised:** 3 February 2025 | **Accepted:** 3 February 2025

Funding: This research was funded by the "Zentrales Innovationsprogramm Mittelstand" (ZIM), grant number KK 5120804KS1.

Keywords: blowing agent mixture | CO_2 | N_2 | open cell content | PLA

ABSTRACT

Polylactid-based (PLA) copolymer foams show a high potential for tissue engineering applications. However, tailored foam properties are required for these applications. As medical authorization is challenging for foams containing chemical modifiers or nucleating agents, tailored foam properties must be achieved by varying process parameters. Employing mixtures of supercritical CO_2 and supercritical N_2 as blowing agents is a promising approach to achieve tailored properties. In this study, the influence of CO_2:N_2 blowing agent mixtures on density, average cell size, open cell content, and storage stability is evaluated for PLA-based copolymer foams suitable for tissue engineering applications. Porosities higher than 90%, which are essential for sufficient cell ingrowth, could be achieved for all blowing agent mixtures. A decreasing average cell size was found for mixtures with low CO_2 content. Improved storage stability and increased open cell contents were achieved for a CO_2 to N_2 volume ratio of 80:20.

1 | Introduction

Polymeric foams have become increasingly important in everyday life, and new applications are constantly emerging. The advantages of foamed products are undeniable and are not only reflected in weight and material savings compared to non-expanded materials. Moreover, tailoring foam morphologies enables specific material properties such as excellent energy absorption, as well as thermal or acoustic insulation [1]. Besides technical applications, foams based on biomaterials, such as Polylactic acid (PLA), play a crucial role in tissue engineering [2]. Depending on the material and its morphology, foams can act as scaffolds for nerve generation, bone tissue restoration, and skin tissue repair, respectively [2].

For scaffold materials, foam properties must be highly tailored. To enable optimized cell ingrowth and fast resorption of the scaffold, a porosity of 90%, high open cell contents (OCC), and cell sizes between 90 and 310 μm are recommended [3–6]. To ensure product usability, a storage stability of several days has to be achieved [4, 5].

Regarding the material, due to their biocompatibility, their beneficial effects on wound healing, and their resorption ability, PLA-based polymers are ideally suited for resorbable soft tissue restoration scaffolds [7, 8]. However, the low melt strength of PLA prevents stable cell growth and thus uniform foam morphologies [9–11]. This low melt strength is also observed for the PLA-based copolymer in this study. Previous studies reported

improved morphologies for PLA-based foams via chemical modification or incorporation of nucleating agents [9, 11–19]. However, the addition of modifiers or additives is challenging for medical approval and might impede residue-free resorption of the scaffold. Instead, desired foam properties must be achieved by varying the foaming parameters.

For material-efficient screening studies, the batch autoclave process is particularly suitable due to its minimal material consumption [20, 21]. Thus, foaming in this study is performed via the pressure drop method in a high-pressure batch autoclave [12].

For this process, crucial parameters are saturation pressure, time, temperature, and the choice of supercritical physical blowing agent (PBA).

Suitable saturation temperatures are essential for low-density foams with desirable morphology. Extreme temperatures lead to unsuitable viscosity and melt strength, preventing expansion or leading to cell coalescence and collapse of the foam structure [19, 22, 23]. For CO_2 and N_2 as PBA, higher pressures increase the dissolved PBA content as well as the nucleation rate while decreasing the viscosity. This results in a decreased foam density and average cell size [12, 24–26]. Foams with similar density but finer cellular morphology exhibit improved dimensional stability, as present stresses on the foam structure are distributed between an increased cell wall surface area [27]. Additionally, foam morphology is influenced by the initial pressure drop rate (PDR) within the first milliseconds upon depressurization of the autoclave [16]. Higher PDRs reduce the energy barrier for nucleation, resulting in a decrease in foam density as well as a decrease in average cell size [16, 28, 29].

Regarding the choice of PBA, predominantly supercritical CO_2 and N_2 have been used in recent years. Both are nonflammable, nontoxic, economical, and environmentally friendly.

CO_2 exhibits a strong plasticizing effect on polymers containing carbonyl groups. This leads to high solubility of the PBA and enables foams with densities below 100 kg m^{-3} [12, 20, 24, 30]. Additionally, the glass transition temperature (T_g) is depressed upon sorption of CO_2. This leads to reduced viscosity and melt strength. Consequently, low densities are achieved at reduced temperatures [31, 32]. For CO_2, a wide range of cell sizes ranging from 10 μm to 1 mm is reported [12]. Due to a synergism between the high diffusivity of CO_2 and its plasticizing effect, pronounced shrinkage is found for the foams during storage [24, 25, 30, 31, 33].

In literature, N_2 is considered less than CO_2 as PBA for PLA-based polymers. For the same amount of solved PBA, N_2 is distinguished by its nucleating effect. This results in an increased cell population density compared to CO_2 [30, 31, 34, 35]. However, due to its significantly reduced solubility, polymer-N_2 systems exhibit high surface tensions, creating a high energy barrier for nucleation and impeding cell growth. Therefore, lower average cell sizes, but higher foam densities are found for N_2 [30, 34–36]. High saturation pressures can help to avoid large non-foamed areas [25, 30]. Due to its lower permeability and absent plasticizing effect, dimensional stability is increased for N_2 compared to CO_2 [25].

To exploit the advantages and compensate for the drawbacks of both PBAs, mixtures of CO_2 and N_2 have been used previously [30, 31, 37]. The solubilities of these mixtures are between the solubilities of the neat PBAs [38]. For the mixtures, significantly lower foam densities compared to N_2 can be realized [12, 30, 33]. Regarding morphology, different results are obtained. For poly(butylene adipate-co-terephthalate) (PBAT) Wang et al. reported lower average cell sizes and narrower cell size distributions for higher shares of N_2 [30]. In contrast, for polystyrene (PS) Wong et al. reported the highest cell population density for a mixture of 75:25% CO_2:N_2 [34]. Compared to N_2, a broader processing window, though without explanation, is reported [34]. Studies on PBAT and thermoplastic polyurethane report improved dimensional stability compared to neat CO_2. This was ascribed to a decreased diffusivity as well as a decreased plasticizing effect of the mixture [30, 33].

Compared to neat PBAs, literature on CO_2:N_2 mixtures is scarce. Especially, the influence of PBA composition on the OCC is not reported. Additionally, morphological results vary across literature, and most studies focus on semicrystalline polymers or polymers with their T_g well above room temperature. Therefore, this study aims to understand the influence of CO_2:N_2 mixtures on the foaming of low T_g PLA-based polymers by evaluating density, average cell size, open cell content, and storage stability for different CO_2:N_2 mixtures.

By tuning process parameters, that is, temperature, pressure, and PBA composition, foams suitable for tissue engineering applications are targeted. In particular, the aim is to achieve a porosity of over 90%, which corresponds to a density of less than 124 kg m^{-3}, while simultaneously aiming for an average cell size of between 90 and 310 μm, high OCC values, and a storage stability of 35 days.

2 | Materials and Methods

2.1 | Materials

An amorphous lactide-based copolymer with a reduced glass transition temperature (T_g) was supplied by Polymedics Innovations GmbH (Kirchheim u. Teck, Germany). Further determined material properties are shown in Table 1.

TABLE 1 | Material properties of the supplied copolymer measured as stated in Sections 2.2.2 and 2.2.3.

Material property	Value
Weight average molecular weight M_w/g mol^{-1}	2.37 * 10^5
Polydispersity index	1.87
Glass transition temperature/°C	34 ± 1
Melt strength/N	0.039 ± 0.015
Zero shear viscosity/Pa s	8.2 * 10^3
Bulk density/kg m^{-3}	1244

As physical blowing agents, neat CO_2 (purity 99.9%), neat N_2 (purity 99.999%), and CO_2:N_2 mixtures of 60:40 vol% (purity 99.9%) and 80:20 vol% (purity 99.9%) were employed, which were supplied by Riessner-Gase GmbH (Lichtenfels, Germany).

2.2 | Methods

2.2.1 | Autoclave Foaming

Foaming was conducted by employing the pressure-drop method on a custom-built autoclave. Depending on the PBA, different setups were chosen (Figure 1). Test specimens with a thickness of 1 mm were produced by hot pressing at 90°C. For foaming, the specimens were placed inside the electrically preheated autoclave, subsequently applying a constant pressure of supercritical PBA. For CO_2 as well as 80:20 and 60:40 CO_2:N_2 mixtures, the pressure was generated by a twin setup of 260D syringe pumps from Teledyne Isco (Thousand Oaks, CA, USA) in constant pressure delivery mode. For the experiments with N_2, the pressure was achieved using a pressure reducer attached to a nitrogen bottle at 200 bar. The PBA was injected into the autoclave chamber by opening valve V1. Saturation pressure and autoclave temperature were varied in an experimental array for all PBA. A saturation time of 30 min was determined by preliminary tests. The foamed samples were stored at room temperature.

2.2.2 | Rheotens

The melt strength was determined using a Rheotens 71.97 device from Göttfert (Buchen, Germany). Prior to the measurement, the copolymer was dried in vacuo at 40°C. After a melting time of 5 min, the melt strand was ejected using an electrically controlled piston (L/D ratio of 26) built in an extensional rheometer from Göttfert (Buchen, Germany), equipped with a round die (L/D ratio of 30 mm/2 mm). The temperature of the extruder was set to 130°C. The measurement wheels exhibited a constant acceleration of 2.4 mm s^{-2} starting from a speed of 15 mm s^{-1} with a strain rate of 30 s^{-1}. The measurement was repeated five times. The melt strength was obtained from the mean force of the last 50 measurement points.

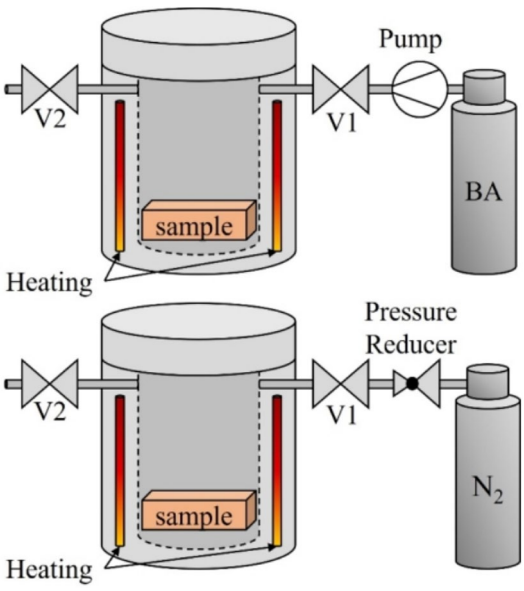

FIGURE 1 | High-pressure autoclave system used for CO_2, CO_2:N_2 mixtures (top) and N_2 (bottom).

2.2.3 | Shear Rheology

Oscillatory shear rheology was conducted with a plate-plate rheometer RDA III from TA Instruments (New Castle, DE, USA) at 130°C with a diameter of 25 mm and a gap of 1 mm under a nitrogen atmosphere. Frequency sweeps were performed from 0.02 to 500 rad s^{-1} (Figure S1). Preceding strain sweeps indicated that a strain of 1% is within the linear viscoelastic range. The hot-pressed samples were dried in vacuo at 40°C before testing. The zero shear viscosity was obtained by fitting data according to the Carreau-Yasuda model [39].

2.2.4 | Differential Scanning Calorimetry (DSC)

To obtain the T_g, DSC measurements were conducted on a DSC 1 from Mettler Toledo (Columbus, OH, USA). Two heating cycles and one cooling cycle with heating rates and cooling rates of 10 K min^{-1} and a nitrogen flow of 50 mL min^{-1} were performed. The holding time between the cycles was 5 min. The data generated in the second heating cycle was used. The experimental temperature ranged from −40°C to 180°C. The analysis was performed threefold.

2.2.5 | Density Evaluation

The initial density of the foams ρ was obtained according to the Archimedes principle on an AG245 balance from Mettler Toledo (Columbus, OH, USA). The measurement was conducted 2 h after foaming. To calculate ρ in kg*m^{-3}, Equation (1) was utilized.

$$\rho = \frac{m(in\ air)}{\left(m(in\ air) - m\left(in\ H_2O\right)\right)} * \rho\left(H_2O\right) \quad (1)$$

With m(in air) and m(in H_2O) as the weights of the foam in air and in de-ionized water, respectively, and ρ(H_2O) as the density of de-ionized water at the measuring temperature.

The porosity Φ was obtained from Equation (2).

$$\Phi = 1 - \frac{\rho_{foam}}{\rho_{bulk}} \quad (2)$$

With $\rho_{bulk} = 1244\ kg\,m^{-3}$ as the density of the unfoamed copolymer and ρ_{foam} as the density of the foam according to Equation (1).

To investigate the long-term stability of the foams, density measurements were conducted multiple times during storage. For further evaluation, ρ_{35} as the density of the foam after 35 days of storage at room temperature was employed.

2.2.6 | Nitrogen Pycnometry

The open-cell content of the samples was evaluated from nitrogen pycnometry on an Ultrafoam 1000 Model UPY-15F from Quantachrome Instruments (Boynton Beach, FL, USA). Since per foaming trial, only one sample is generated, the OCC could not be measured directly. This is because density must be determined beforehand with the Archimedes method, leading to remaining water inside the foam that distorts pycnometry results. Instead, the initial density ρ was measured according to Equation (1). On the following day, the dried sample was used for pycnometry, wherefore sample mass and volume must be set. The sample mass m was obtained before the measurement. For the sample volume, the initial volume V_{ini} in cm^3 was used, which is calculated according to Equation (3).

$$V_{ini} = \frac{m}{\rho} \tag{3}$$

With m and V_{ini}, as well as the calculations mentioned in the ASTM standard D6226, the pycnometer calculates an OCC value, which here is referred to as OCC_{hyp}.

For each sample, a maximum of seven runs was performed for the OCC measurement, whereby the output value complied with the average of the last three runs. Alternatively, if the standard deviation reached 0.005%, the measurement was terminated early. To obtain the true OCC, the density was measured once more, obtaining the true foam density ρ_{true} and consequently the true sample volume present during pycnometry V_{true}. The true OCC in % was calculated by Equation (4).

$$OCC = \frac{\left(V_{ini} * \left(OCC_{hyp} - 1\right) + V_{true}\right)}{V_{true}} \tag{4}$$

with

$$V_{true} = \frac{m}{\rho_{true}} \tag{5}$$

2.2.7 | Scanning Electron Microscopy (SEM)

Foam morphology was evaluated by scanning electron microscopy (SEM) on a Zeiss Leo 1530 from Carl Zeiss AG (Oberkochen, Germany), which is equipped with a tungsten cathode and a SE1 detector. The samples were cut in half and sputtered with gold. Average cell size and cell size distribution were determined from SEM images. Nucleation density N in cells*cm^{-3} was evaluated by Equation (6).

$$N = \left(\frac{N_0}{A}\right)^{\frac{3}{2}} * VER \tag{6}$$

with N_0 as the number of cells in a specified area A and VER as the volume expansion ratio.

VER is calculated according to Equation (7).

$$VER = \frac{\rho_{bulk}}{\rho_{foam}} \tag{7}$$

2.2.8 | Gel Permeation Chromatography (GPC)

The weight average molecular weight M_w was determined utilizing a Tosoh EcoSEC pump from Tosoh Bioscience (Tokyo, Japan) at 23°C in a PSS SDV Linear XL gel column with a particle size of 5 µm and a porosity of 100 Å. Chloroform was used as the mobile phase with a sample concentration of 1 g L^{-1}. A flow rate of 0.5 mL min^{-1} was applied. Conventional calibration against polystyrene standards was used.

3 | Results and Discussion

3.1 | Foaming With CO_2

Foam density over a wide parameter range is depicted in Figure 2. An ideal processing window, describing densities below 124 kg m^{-3}, was obtained for temperatures between 35°C and 70°C and pressures between 80 and 140 bar. Temperature and pressure limits of the processing window are known in the literature and described elsewhere [19, 22, 23, 25, 29, 30, 40, 41]. Densities below 25 kg m^{-3} could be achieved at 55°C to 65°C and 80 to 120 bar.

OCC over the same parameter range is depicted in Figure 3. Mostly, OCC below 25% was realized within the above-described processing window. OCC values between 25% and 75% were realized outside the processing window and for temperatures of 65°C. The OCC is dependent on viscosity, melt strength, cell density, as well as VER of a given polymer. As seen in Figures 2 and 3 a high VER, equaling low densities, and a high OCC are mostly mutually exclusive for the given copolymer. Further, low OCC values are present for parameters leading to high cell density (Table 2). Thus, thin cell walls resulting from high expansion or a high cell density do not lead to cell wall rupture for this copolymer. Instead, viscosity and melt strength that are adjusted by the saturation temperature seem to be the most crucial factors influencing the OCC. For elevated temperatures, increased OCC values are found, as the melt strength of the polymer is reduced until cell walls cannot withstand the stress during stretching and rupture occurs. As this phenomenon is often accompanied

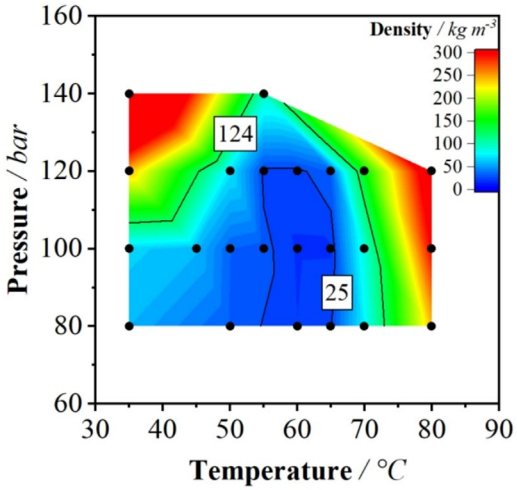

FIGURE 2 | Contour plot of density against temperature and pressure; Measured data shown as points; Density limits of 124 and 25 kg m^{-3} shown as lines.

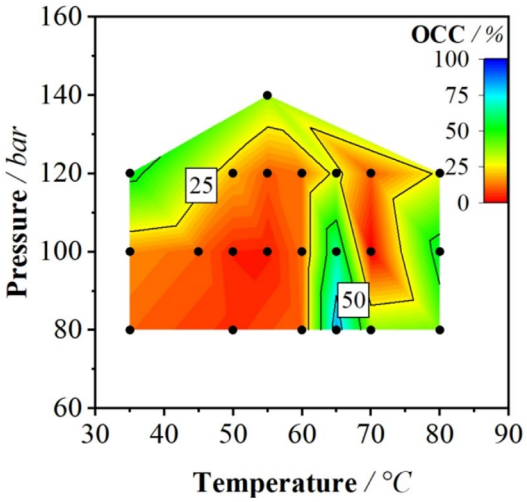

FIGURE 3 | Contour plot of OCC against temperature and pressure; Measured data shown as points; OCC limits of 25% and 50% shown as lines.

TABLE 2 | Foam characteristics for foaming with CO_2 at 65°C at 80, 100, and 120 bar.

	80 bar	100 bar	120 bar
Initial density/kg m^{-3}	19	19	22
Density after 35 days/ kg m^{-3}	129	66	47
Average cell size/μm	136 ± 30	62 ± 14	48 ± 11
Volume expansion ratio	66	64	56
Nucleation density/10^6 cells cm^{-3}	26	246	410
OCC/%	83	65	28

by a coarsened, non-uniform morphology, this mechanism of cell opening is not desired. Alternatively, for low temperatures in combination with high pressures, severe pressure-induced cooling takes place during the autoclave depressurization. This results in a fast increase in viscosity that leads to brittle cell wall fracture and high OCC. Simultaneously, improved foam morphologies are realized under these conditions as the high viscosity and melt strength stabilize the foam structure.

To investigate and verify the influence of pressure on the foam morphology, cross-sections of the foams obtained at a constant temperature of 65°C but varying pressures were compared via SEM (Figure 4). While foam density is only influenced slightly by pressure (Table 2), morphology is highly dependent on it (Figure 4). For higher pressures, significantly increased nucleation densities resulting in a reduced average cell size and a narrower cell size distribution were observed. This results from higher pressures leading to a higher sorption of CO_2 and a decreased PBA-polymer interface tension. Thus, homogeneous nucleation is promoted [25, 29, 30]. From pycnometry, a reduction in the OCC was visible for higher pressures (Table 2). However, comparison to SEM images suggests that especially for the foam obtained at 80 bar, the high OCC value from pycnometry seems to overestimate the number of truly open

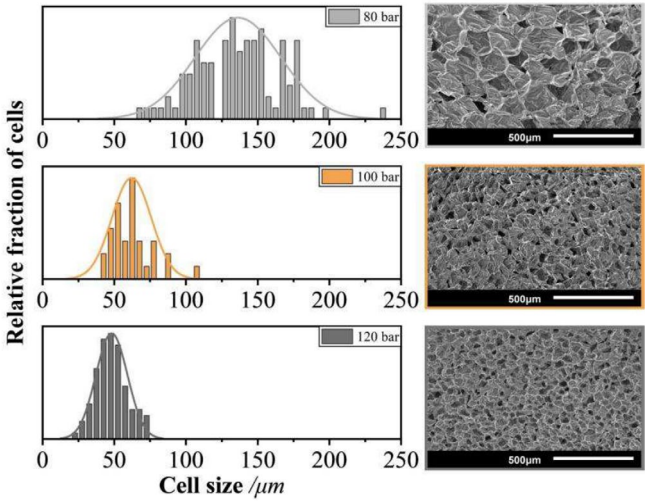

FIGURE 4 | Histograms (left) and corresponding SEM images (right) for foaming with CO_2 at 65°C and 80 bar (top), 100 bar (middle), and 120 bar (bottom).

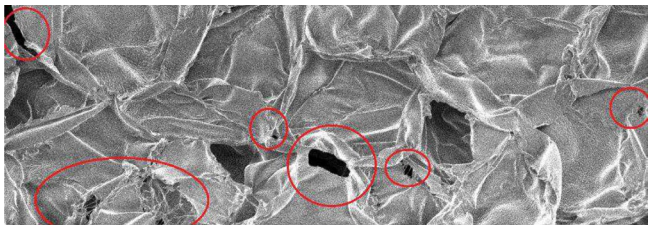

FIGURE 5 | Higher magnification SEM image of the foam achieved at 65°C and 80 bar. Small intercellular openings marked in red circles.

cells. However, in higher magnification SEM images, small cell-interconnecting holes (Figure 5) are visible, which lead to the high OCC number in pycnometry.

As a next step, the influence of saturation pressure on the dimensional stability of the foams was examined (Table 2, Figure 6).

As evident from Figure 6, a density increase was observed for all foams during storage. The increase within the first day was the highest. After 35 days, the further change in density was only minor. As 35 days is a sufficient storage time for foams in tissue engineering, the percental density increase after 35 days was examined in more detail. There, the shrinkage effect is more pronounced for lower saturation pressures. This phenomenon is attributed to the reduced average cell size at higher saturation pressures, allowing stresses on the foam structure to be distributed between a higher number of cell walls and an increased cell wall surface area [27].

3.2 | Foaming With CO_2:N_2 Mixtures

3.2.1 | Influence on Processing Window

The influence of the PBA mixture on the processing window is shown in Figure 7.

For temperatures below 160°C, no sufficient expansion was found for N_2. For higher temperatures, foams with densities as low as

200 kg m^{-3} but coarse morphology were realized (Figure S1). This can be attributed to the low solubility and the absent plasticizing effect of N_2. N_2 exhibits a greater nucleating effect and expansion ratio for the same amount of PBA dissolved compared to CO_2 [30, 35]. However, this advantage is overruled by its significantly lower solubility, which decreases the nucleation density substantially. As a result, only a few bubble nuclei are formed. Regarding saturation temperature and plasticizing effect, for CO_2, saturation takes place at lower temperatures, and the foam structure is rapidly stabilized during depressurization. This stabilization occurs as the outward diffusion of CO_2 reduces the plasticizing effect on the polymer, rapidly increasing both T_g and viscosity.

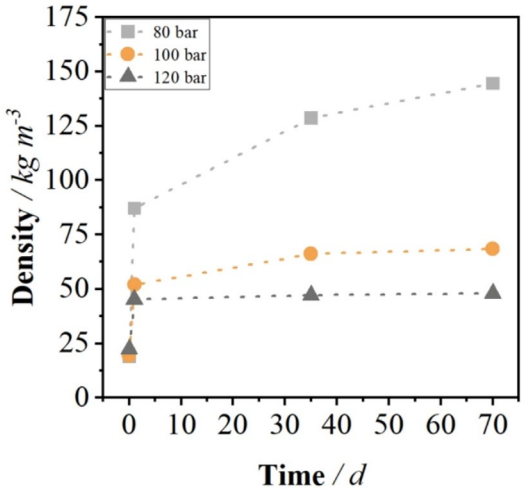

FIGURE 6 | Influence of saturation pressure on density increase for foaming with CO_2 at 65°C.

Consequently, cell coalescence and collapse of the foam structure are prevented effectively. In contrast, this stabilization mechanism does not occur with N_2. Instead, the low viscosity induced by high saturation temperatures leads to an undesired morphology as observed in this study. Therefore, foaming with 100% N_2 is not expedient for the present copolymer.

For both CO_2:N_2 mixtures, stable processing windows were observed. For the mixtures, the processing windows are not linearly narrowed for lower CO_2 shares, as for 80:20 CO_2:N_2 it is widened. In contrast, for 60:40 CO_2:N_2, the window becomes smaller as expansion is hindered at temperatures below 50°C. This hindrance is due to the decreased solubility of this PBA mixture, which results from the high share of N_2. For 80:20 CO_2:N_2, the widened processing window results from successful expansion at low temperatures and high pressures. This originates from two factors: a small decrease in the above-mentioned stabilizing effect, which is caused by the share of N_2 in the PBA mixture, and a decreased cooling effect during depressurization. Both factors allow viscosities to remain low, thus increasing expansion times and consequently leading to low densities.

The decreased cooling effect can be proven by comparing the time-dependent temperature profiles during depressurization (Figure 8). It must be noted that for the present autoclave system, the measurement of the built-in thermometer is delayed. Hence, no quantitative temperature data can be obtained, as the measured temperature drop is significantly lower than the actual one. As a reference, solid CO_2 was found in the autoclave after depressurization for 100% CO_2, which highlights temperatures below −56.4°C [40, 42]. Nevertheless, the

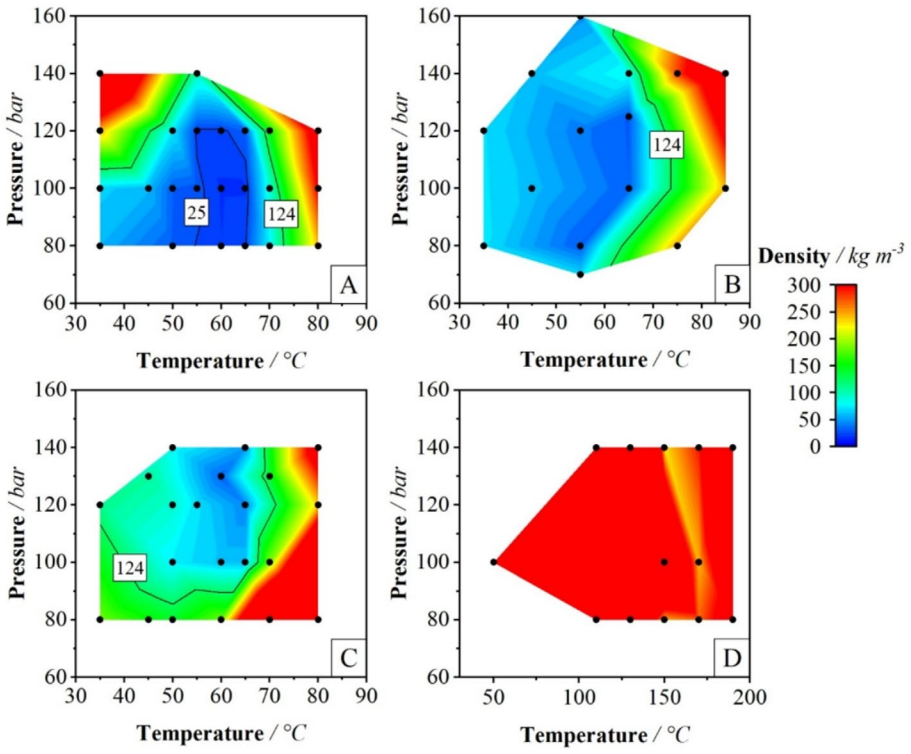

FIGURE 7 | Contour plots of density against temperature and pressure for CO_2 (A), 80:20 (B) and 60:40 CO_2:N_2 (C), and N_2 (D); Measured data shown as points; Density limits of 124 and 25 kg/m^3 shown as lines.

relative temperature differences between the PBA mixtures can be analyzed. It is evident that with an increasing share of N_2, the temperature drop is reduced. Thus, the temperature of the system remains above the T_g of the copolymer for a longer period. This allows for continued expansion, and lower densities are realized.

Additionally, the pressure limits of the processing window shift towards higher values. While sufficiently low densities can be achieved at 60 bar for CO_2, a minimum of 80 and 100 bar is required for 80:20 and 60:40 CO_2:N_2, respectively, as higher pressures are necessary to compensate for the reduced solubility of the PBA mixtures compared to CO_2 [35].

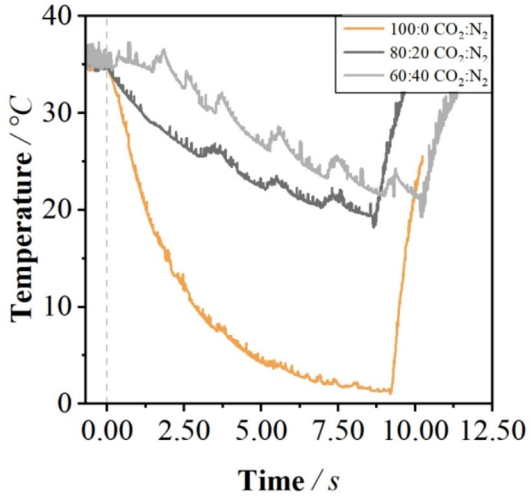

FIGURE 8 | Pressure-drop-induced temperature profile of the autoclave system for saturation conditions of 35°C and 120 bar.

3.2.2 | Influence on Morphology

As no decent expansion was generated for N_2, this PBA is not considered for the following investigations. For the remaining blowing agents, the effect of the PBA ratio on the OCC was evaluated (Figure 9).

Similar to the foams produced with neat CO_2, low density and high OCC are mostly mutually exclusive for 60:40 CO_2:N_2. Further, for none of the PBA mixtures, high OCC values were obtained at low temperatures in combination with high pressures. The reason for this is the reduced pressure-drop-induced cooling for the PBA mixtures (Figure 8) that prevents brittle cell wall fracture.

When foamed outside the ideal processing window, all PBA mixtures lead to cell wall fracture due to low viscosity and melt strength, resulting in high OCC and high foam density. It is noteworthy that for 80:20 CO_2:N_2 within a broad parameter range, high OCC values were obtained, while simultaneously maintaining low densities. This effect is caused by a slightly decreased stabilization effect in combination with a low pressure-drop-induced cooling at small saturation pressures (see also Section 3.2.1). Thus, prolonged expansion is possible during depressurization, and cell wall rupture occurs. Nevertheless, the foam is still stabilized. Consequently, although this cell wall opening is not due to brittle fracture, a narrow cell size distribution and suitable morphology were realized (Figure 10).

Regarding foam morphology, for identical saturation conditions, an increased share of N_2 results in decreased nucleation density as well as increased average cell size and foam density (Table 3). Additionally, the cell size distribution was broadened, especially for 60:40 CO_2:N_2 (Figure 10).

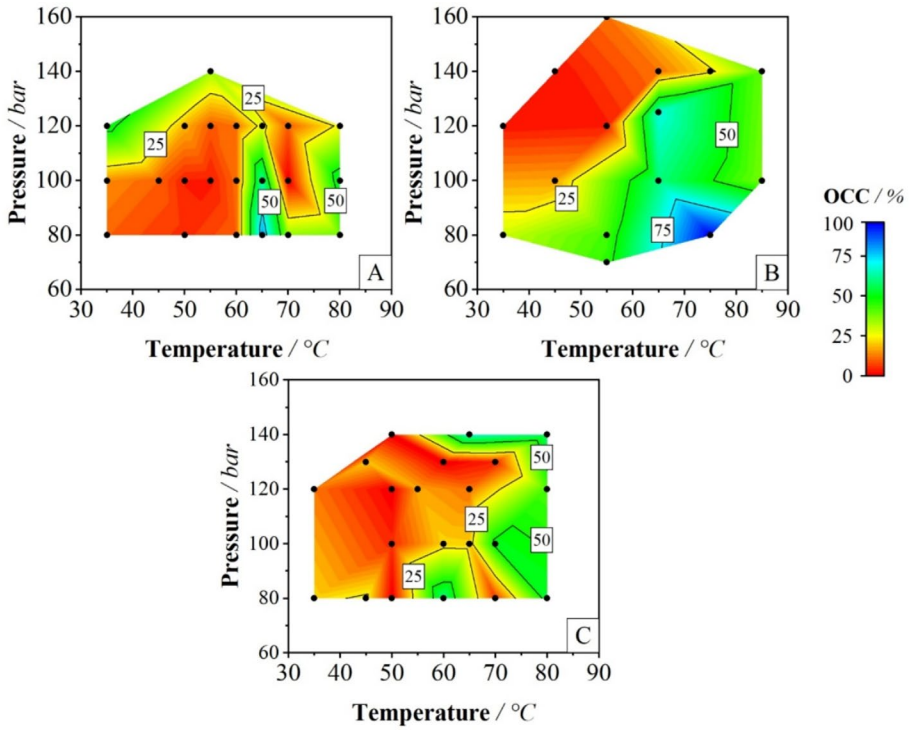

FIGURE 9 | Contour plots of OCC against temperature and pressure for CO_2 (A), 80:20 (B) and 60:40 CO_2:N_2 (C); Measured data shown as points; OCC limits of 25%, 50%, and 75% shown as lines.

Regarding average cell size, results deviate from literature, where either smaller cell sizes exist increase of the N_2 share, or a synergistic effect of CO_2 and N_2 is proclaimed, which leads to the lowest average cell sizes for a mixture of 75:25% CO_2:N_2

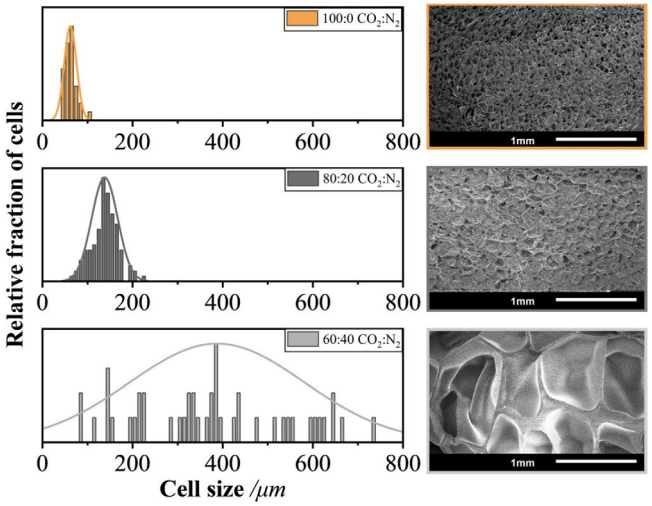

FIGURE 10 | Histograms (left) and corresponding SEM images (right) for CO_2 (top), 80:20 (middle), and 60:40 CO_2:N_2 (bottom) at 65°C and 100 bar.

TABLE 3 | Foam characteristics for CO_2, 80:20, and 60:40 CO_2:N_2 at 65°C and 100 bar.

	100% CO_2	80:20 CO_2:N_2	60:40 CO_2:N_2
Initial density/kg m^{-3}	18	32	61
Density after 35 days/ kg m^{-3}	74	78	283
Average cell size/μm	62	138	387
Volume expansion ratio	69	40	20
Nucleation density/10^6 cells cm^{-3}	246	224	0.23
OCC/%	65	60	21

[30, 34]. The positive correlation between N_2 share and average cell size, as well as the inverse correlation between N_2 share and nucleation density observed in this study, may be attributed to multiple factors. These include decreased solubility, decreased stabilization effect, decreased pressure-drop-induced cooling, and a lower PDR of the PBA mixture compared to 100% CO_2. The review of these factors reveals that, regarding the latter factor, the total time until depressurization is significantly longer for 60:40 CO_2:N_2 compared to CO_2 and 80:20 CO_2:N_2 (Figure 11A).

However, the initial PDR within the first milliseconds is equal for all PBA mixtures. Since cell nucleation is reported [16] to occur within this first timeframe, it is likely not affected by the variation of the PBA mixture at these saturation conditions. Additionally, the pressure-induced cooling effect is similar for these process conditions for all PBA mixtures (Figure 11B).

This leads to the conclusion that a decreased stabilization effect and a decreased solubility of the PBA mixtures are the driving factors for morphology development. Due to the decreased stabilization effect, viscosity increases more slowly for the PBA mixtures during depressurization, and consequently, expansion ratio and cell coalescence increase. Additionally, the solubility of the PBA mixtures is reduced compared to CO_2 [38]. This results in a decreased nucleation density, leading to fewer larger cells. However, the exact solubility limits of the neat PBA and their mixtures cannot be measured in this study. Solubility is typically measured by loading the polymer with gas in an autoclave and measuring the weight increase of the sample after it is removed. However, this is only applicable to polymers that do not foam at room temperature [9].

3.2.3 | Influence on Stability

No linear correlation between stability and PBA composition was found (Figure 12). However, the influence of the PBA mixture cannot be assessed in isolation as a change of the PBA causes a variation in foam morphology. To achieve comparable morphology, saturation conditions must be altered for the respective PBA mixtures. Since the influence of deviating morphology on dimensional stability can be more accurately predicted than the influence of differing saturation pressures, foams obtained at the same saturation conditions were compared. For the foams produced with CO_2 and 80:20 CO_2:N_2, the average cell size and OCC are comparable.

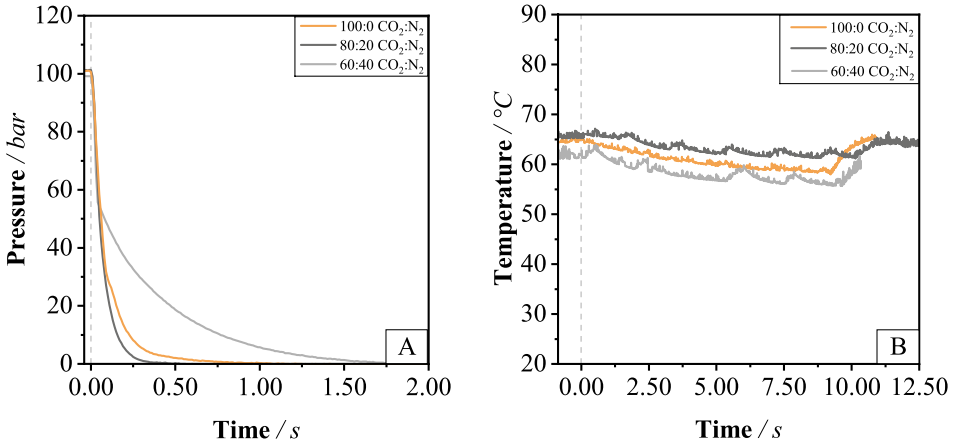

FIGURE 11 | Pressure drop rates (A) and cooling effect (B) upon depressurization with different PBA mixtures at 65°C, 100 bar.

In contrast, a significantly increased average cell size and reduced OCC were observed for 60:40 CO_2:N_2. These morphology deviations influence the dimensional stability of the foam. Regarding the effect of cell size on dimensional stability, its impact remains a topic of discussion in the literature. Some studies report that dimensional stability decreases as average cell size increases, while others suggest the opposite effect [27, 43]. In this study, decreased stability was found for the foam with highly increased average cell size and decreased OCC. We attribute this to a combination of several factors. Due to the low OCC, many cells are isolated from the outside and experience negative pressure as residual PBA diffuses outward post-foaming. As the average cell size is high, few cell walls are present to withstand the stress induced by the outward diffusion of the PBA. Additionally, the proximity of the T_g of copolymer to the storage temperature results in softened cell walls. Thus, under these conditions, large, closed-cell structures exhibit reduced dimensional stability.

For CO_2 and 80:20 CO_2:N_2, morphology is comparable. For 80:20 CO_2:N_2, the relative density increase after 35 days was reduced from 306% to 146%, which equals a relative reduction of 52% compared to CO_2. This effect can be ascribed to two factors. Firstly, a lower outward diffusion rate is reported for CO_2:N_2 mixtures compared to CO_2. As a consequence, negative cell pressure is minimized [33]. Secondly, due to the reduced amount of CO_2, the plasticizing effect is reduced. Consequently, cell walls have more strength and can withstand a greater amount of stress, leading to improved dimensional stability of the foam structure.

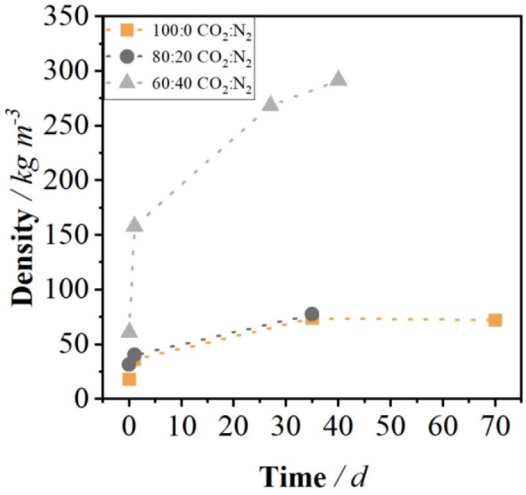

FIGURE 12 | Influence of PBA ratio on density increase for CO_2, 80:20, and 60:40 CO_2:N2 at 65°C with 100 bar.

3.3 | Processing—Property Correlations

To confirm the results, the processing parameters temperature, pressure, and share of CO_2 (100%, 80%, 60%) were correlated with the foam properties. Pearson's correlation coefficients R_p were calculated using Python 3.9.12. Further information on their calculation can be found in the Supporting Information. The correlation analysis (Figure 13) reveals a moderately negative correlation between the share of CO_2 and the initial density ($R_p = -0.63$) as well as average cell size ($R_p = -0.59$). However, a moderately positive correlation with nucleation density was found ($R_p = 0.66$). This correlation verifies that increasing the share of CO_2 leads to a decrease in average cell size. The negative correlation with density implies that despite achieving low densities for all PBA mixtures under certain conditions, only for 100% CO_2 were extremely low densities (< 24 kg m^{-3}) found. This likely overrules other effects such as the wider processing window for 80:20 CO_2:N_2. Between the share of CO_2 and OCC ($R_p = 0.25$) as well as the share of CO_2 and relative density increase after 35 days ($R_P = -0.33$) only weak negative correlations were found. This is due to the non-linearity of correlation, as the highest OCC and stability were found for 80:20 CO_2:N_2.

4 | Conclusion

This study showed that an alteration in process parameters and physical blowing agents leads to differing foam densities and morphologies.

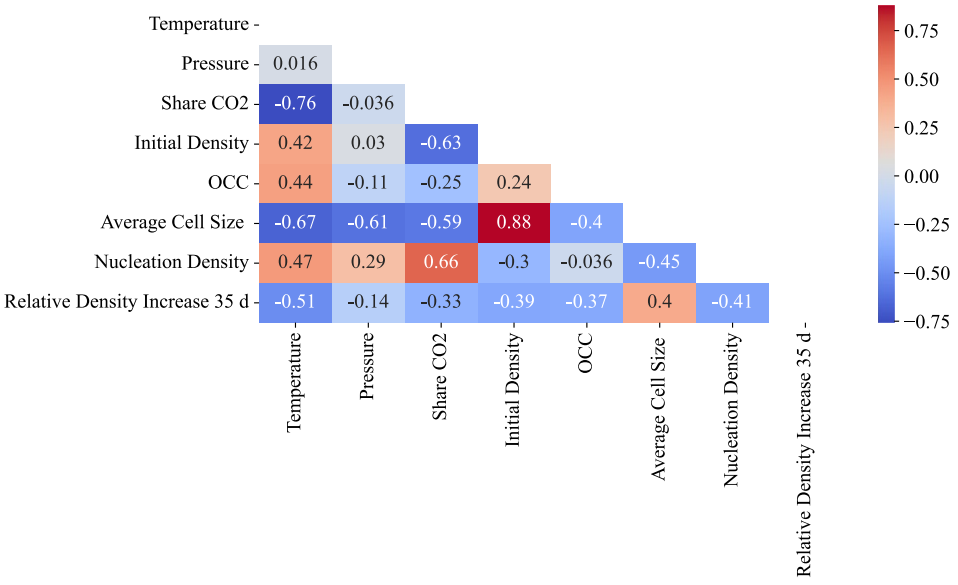

FIGURE 13 | Pearson's correlation coefficients of processing parameters and foam properties.

Regarding the PBA, a change from neat CO_2 to neat N_2 led to limited expansion and non-uniform cell morphologies. For neat CO_2, 80:20 and 60:40 CO_2:N_2, foams with porosities above 90% were achieved. Decreased pressure-drop-induced cooling was found for the CO_2:N_2 mixtures. The lower plasticization of PBA mixtures, in combination with their decreased stabilizing effect from the pressure drop, enabled expansion at low temperatures and high pressures, resulting in a broadened processing window for 80:20 CO_2:N_2.

Regarding OCC for 80:20 CO_2:N_2, it was possible to achieve high OCC while maintaining low foam densities. In terms of morphology, average cell size was increased for the PBA mixtures compared to CO_2. For 80:20 CO_2:N_2, improved stability was found compared to CO_2, which was ascribed to a synergistic effect between the reduced plasticizing effect and the decreased diffusivity of the PBA mixture.

Regarding the desired foam characteristics, foam structures could be generated for 80:20 CO_2:N_2 that simultaneously exhibited porosities above 90%, sufficiently high OCC, sufficient storage stability as well as cell sizes in the range of 90 to 310 µm. Tuning PBA composition can thus be considered a highly promising tool to achieve tailored foam structures.

Acknowledgments

The authors would like to acknowledge the Bavarian Polymer Institute (BPI) for providing access to GPC and SEM measurements.

Conflicts of Interest

The authors declare no conflicts of interest.

Data Availability Statement

Data will be made available upon request.

References

1. R. K. Gupta, ed., *Polymeric Foams: Applications of Polymeric Foams (Volume 2)*, 2nd ed. (ACS Symposium Series, 2023).

2. P. A. Netti, ed., *Biomedical Foams for Tissue Engineering Applications* (Woodhead Publishing, 2014).

3. Y. I. Heit, P. Dastouri, D. L. Helm, et al., "Foam Pore Size Is a Critical Interface Parameter of Suction-Based Wound Healing Devices," *Plastic and Reconstructive Surgery* 129, no. 3 (2012): 589–597, https://doi.org/10.1097/PRS.0b013e3182402c89.

4. S. Ebnesajjad, *Handbook of Biopolymers and Biodegradable Plastics: Properties, Processing and Applications* (William Andrew Publishing, 2012), https://doi.org/10.1016/C2011-0-07342-8.

5. M. R. MacEwan, S. MacEwan, T. R. Kovacs, and J. Batts, "What Makes the Optimal Wound Healing Material? A Review of Current Science and Introduction of a Synthetic Nanofabricated Wound Care Scaffold," *Cureus* 9, no. 10 (2017): e1736, https://doi.org/10.7759/CUREUS.1736.

6. L. E. Freed, G. Vunjak-Novakovic, R. J. Biron, et al., "Biodegradable Polymer Scaffolds for Tissue Engineering," *Nature Biotechnology* 12, no. 7 (1994): 689–693.

7. K. Gürünlüoğlu, M. Demircan, A. Koç, et al., "The Effects of Different Burn Dressings on Length of Telomere and Expression of Telomerase in Children With Thermal Burns," *Journal of Burn Care & Research* 40, no. 3 (2019): 302–311, https://doi.org/10.1093/jbcr/irz019.

8. K. Gürünlüoğlu, M. Demircan, A. Taşçı, et al., "The Effects of Two Different Burn Dressings on Serum Oxidative Stress Indicators in Children With Partial Burn," *Journal of Burn Care & Research* 40, no. 4 (2019): 444–450, https://doi.org/10.1093/jbcr/irz037.

9. C. Brütting, J. Dreier, C. Bonten, V. Altstädt, and H. Ruckdäschel, "Amorphous Polylactide Bead Foam–Effect of Talc and Chain Extension on Foaming Behavior and Compression Properties," *Journal of Renewable Materials* 9, no. 11 (2021): 1859–1868, https://doi.org/10.32604/jrm.2021.016244.

10. M. Nofar, A. Ameli, and C. B. Park, "A Novel Technology to Manufacture Biodegradable Polylactide Bead Foam Products," *Materials and Design* 83 (2015): 413–421, https://doi.org/10.1016/j.matdes.2015.06.052.

11. S. M. Castellón, T. Standau, V. Altstädt, and C. Bonten, "Effect of the Chemical Modification on the Thermal and Rheological Properties of Different Polylactides for Foaming," *AIP Conference Proceedings* 2205 (2020): 020068, https://doi.org/10.1063/1.5142983.

12. T. Standau, C. Zhao, S. M. Castellón, C. Bonten, and V. Altstädt, "Chemical Modification and Foam Processing of Polylactide (PLA)," *Polymers* 11, no. 2 (2019): 306, https://doi.org/10.3390/polym11020306.

13. Y. Di, S. Iannace, E. Di Maio, and L. Nicolais, "Reactively Modified Poly (Lactic Acid): Properties and Foam Processing," *Macromolecular Materials and Engineering* 290, no. 11 (2005): 1083–1090, https://doi.org/10.1002/mame.200500115.

14. D. Dörr, T. Standau, S. M. Castellón, C. Bonten, and V. Altstädt, "Rheology in the Presence of Carbon Dioxide (CO2) to Study the Melt Behavior of Chemically Modified Polylactide (PLA)," *Polymers* 12, no. 5 (2020): 1–10, https://doi.org/10.3390/POLYM12051108.

15. T. Standau, S. Goettermann, S. Weinmann, C. Bonten, V. Altstädt, and E. Di Maio, "Autoclave Foaming of Chemically Modified Polylactide," *Journal of Cellular Plastics* 53, no. 5 (2017): 481–489, https://doi.org/10.1177/0021955X16670588.

16. T. Standau, H. Long, S. M. Castellón, C. Brütting, C. Bonten, and V. Altstädt, "Evaluation of the Zero Shear Viscosity, the D-Content and Processing Conditions as Foam Relevant Parameters for Autoclave Foaming of Standard Polylactide (PLA)," *Materials* 13, no. 6 (2020): 1371, https://doi.org/10.3390/ma13061371.

17. Y. Liu, H. Cao, L. Ye, P. Coates, F. Caton-Rose, and X. Zhao, "Long-Chain Branched Poly(Lactic Acid)- b-Poly(Lactide- Co-Caprolactone): Structure, Viscoelastic Behavior, and Triple-Shape Memory Effect as Smart Bone Fixation Material," *Industrial and Engineering Chemistry Research* 59, no. 10 (2020): 4524–4532, https://doi.org/10.1021/acs.iecr.9b06514.

18. J. A. Villamil Jiménez, N. Le Moigne, J.-C. Bénézet, et al., "Foaming of PLA Composites by Supercritical Fluid-Assisted Processes: A Review," *Molecules* 25, no. 15 (2020): 3408, https://doi.org/10.3390/molecules25153408.

19. P. Tiwary, C. B. Park, and M. Kontopoulou, "Transition From Microcellular to Nanocellular PLA Foams by Controlling Viscosity, Branching and Crystallization," *European Polymer Journal* 91, no. March (2017): 283–296, https://doi.org/10.1016/j.eurpolymj.2017.04.010.

20. C. Okolieocha, D. Raps, K. Subramaniam, and V. Altstädt, "Microcellular to Nanocellular Polymer Foams: Progress (2004-2015) and Future Directions - A Review," *European Polymer Journal* 73 (2015): 500–519, https://doi.org/10.1016/j.eurpolymj.2015.11.001.

21. M. Altan, "Thermoplastic Foams: Processing, Manufacturing, and Characterization," in *Recent Research in Polymerization*, ed. N. Cankaya (InTech, 2018), 117–137, https://doi.org/10.5772/intechopen.71083.

22. N. Najafi, M. C. Heuzey, P. J. Carreau, D. Therriault, and C. B. Park, "Rheological and Foaming Behavior of Linear and Branched

Polylactides," *Rheologica Acta* 53, no. 10–11 (2014): 779–790, https://doi.org/10.1007/s00397-014-0801-3.

23. Y. Wang, C. Zhang, S. Han, et al., "Morphological Evolution From Open Cells to Reticulated Structures in Moderately Branched Polybutylene Terephthalate Foamed Using Supercritical CO_2," *Advanced Engineering Materials* 24, no. 3 (2022): 1–13, https://doi.org/10.1002/adem.202101102.

24. J. Reignier, R. Gendron, and M. F. Champagne, "Extrusion Foaming of Poly(Lactic Acid) Blown With CO_2: Toward 100% Green Material," *Cellular Polymers* 26, no. 2 (2007): 83–115, https://doi.org/10.1177/026248930702600202.

25. H. Zhang, T. Liu, B. Li, et al., "Foaming and Dimensional Stability of LDPE Foams With N2, CO_2, i-C4H10 and CO_2 - N2 Mixtures as Blowing Agents," *Journal of Supercritical Fluids* 164 (2020): 104930, https://doi.org/10.1016/j.supflu.2020.104930.

26. K. Wilczynski, *Rheology in Polymer Processing*, 1st ed. (Carl Hanser Verlag, 2021).

27. Z. G. Xu, J. W. Fu, T. J. Luo, and Y. S. Yang, "Effects of Cell Size on Quasi-Static Compressive Properties of Mg Alloy Foams," *Materials and Design* 34 (2012): 40–44, https://doi.org/10.1016/j.matdes.2011.07.066.

28. X. Xu, C. B. Park, D. Xu, and R. Pop-Iliev, "Effects of Die Geometry on Cell Nucleation of PS Foams Blown With CO_2," *Polymer Engineering and Science* 43, no. 7 (2003): 1378–1390.

29. S. N. S. Leung, "Mechanism of Cell Nucleation, Growth and Coarsening in Plastic Foaming: Theory, Simulation and Experiments," Toronto (2009).

30. Z. Wang, J. Zhao, G. Wang, et al., "Lightweight, Low-Shrinkage and High Elastic Poly(Butylene Adipate-Co-Terephthalate) Foams Achieved by Microcellular Foaming Using N_2 & CO_2 as CO-Blowing Agents," *Journal of CO_2 Utilization* 64, no. July (2022): 102149, https://doi.org/10.1016/j.jcou.2022.102149.

31. E. Di Maio, G. Mensitieri, S. Iannace, L. Nicolais, W. Li, and R. W. Flumerfelt, "Structure Optimization of Polycaprolactone Foams by Using Mixtures of CO_2 and N 2 as Blowing Agents," *Polymer Engineering and Science* 45, no. 3 (2005): 432–441, https://doi.org/10.1002/pen.20289.

32. S. Zepnik, S. Kabasci, R. Kopitzky, H. J. Radusch, and T. Wodke, "Extensional Flow Properties of Externally Plasticized Cellulose Acetate: Influence of Plasticizer Content," *Polymers (Basel)* 5, no. 3 (2013): 873–889, https://doi.org/10.3390/polym5030873.

33. W. P. Zhong, Z. Yu, T. Zhu, Y. Zhao, A. D. Phule, and Z. X. Zhang, "Influence of Different Ratio of CO_2/N_2 and Foaming Additives on Supercritical Foaming of Expanded Thermoplastic Polyurethane," *Express Polymer Letters* 16, no. 3 (2022): 318–336, https://doi.org/10.3144/EXPRESSPOLYMLETT.2022.24.

34. A. Wong, L. H. Mark, M. M. Hasan, and C. B. Park, "The Synergy of Supercritical CO_2 and Supercritical N2 in Foaming of Polystyrene for Cell Nucleation," *Journal of Supercritical Fluids* 90 (2014): 35–43, https://doi.org/10.1016/j.supflu.2014.03.001.

35. J. W. S. Lee and C. B. Park, "Use of Nitrogen as a Blowing Agent for the Production of Fine-Celled High-Density Polyethylene Foams," *Macromolecular Materials and Engineering* 291, no. 10 (2006): 1233–1244, https://doi.org/10.1002/mame.200600203.

36. Y. Sun, Y. Ueda, H. Suganaga, M. Haruki, S. I. Kihara, and S. Takishima, "Pressure Drop Threshold in the Foaming of Low-Density Polyethylene, Polystyrene, and Polypropylene Using CO_2 and N_2 as Foaming Agents," *Journal of Supercritical Fluids* 103 (2015): 38–47, https://doi.org/10.1016/j.supflu.2015.04.027.

37. D. Tammaro, *Fundamentals of Cell Opening in Polymer Foaming* (Neaples Federico II, 2016).

38. M. M. Hasan, "A Systematic Study of Solubility of Physical Blowing Agents and Their Blends in Polymers and Their Nanocomposites," University of Toronto (2013), https://tspace.library.utoronto.ca/bitstream/1807/68987/1/Hasan_Mohammad_M_201311_PhD_Thesis.pdf.

39. P. J. Carreau, D. C. R. Da Kee, and R. P. Chhabra, *Rheology of Polymeric Systems*, 1st ed. (Hanser Publishers, 1997).

40. M. Dippold and H. Ruckdäschel, "Influence of Pressure-Induced Temperature Drop on the Foaming Behavior of Amorphous Polylactide (PLA) During Autoclave Foaming With Supercritical CO_2," *Journal of Supercritical Fluids* 190 (2022): 105734, https://doi.org/10.1016/j.supflu.2022.105734.

41. N. S. Oliveira, J. Dorgan, A. P. Coutinho, A. Ferreira, J. L. Daridon, and I. M. Marrucho, "Gas Solubility of Carbon Dioxide in Poly(Lactic Acid) at High Pressures: Thermal Treatment Effect," *Journal of Polymer Science Part B: Polymer Physics* 45, no. 5 (2007): 616–625, https://doi.org/10.1002/polb.

42. R. Blanes-Rex, E. P. A. Fernández, and F. Guzmán, "On the Triple Point Temperature of CO2," *Cryogenics (Guildf)* 22, no. 3 (1982): 113–114, https://doi.org/10.1016/0011-2275(82)90105-9.

43. H. Yu, Z. Guo, B. Li, G. Yao, H. Luo, and Y. Liu, "Research Into the Effect of Cell Diameter of Aluminum Foam on Its Compressive and Energy Absorption Properties," *Materials Science and Engineering A* 454 (2007): 542–546, https://doi.org/10.1016/j.msea.2006.11.091.

Supporting Information

Additional supporting information can be found online in the Supporting Information section.